fluids

MDPI

Article

Experimental Investigation of the Performance of a Novel Ejector–Diffuser System with Different Supersonic Nozzle Arrays

Dachuan Xu [1,2], Yunsong Gu [1], Wei Li [3] and Jingxiang Chen [2,*]

[1] College of Aerospace Engineering, Nanjing University of Aeronautics and Astronautics, Nanjing 210016, China
[2] State Key Laboratory of Aerodynamics, China Aerodynamics Research and Development Center, Mianyang 621000, China
[3] Department of Energy Engineering, Zhejiang University, Hangzhou 310027, China
* Correspondence: jingxiangchen@zju.edu.cn

Abstract: The supersonic–supersonic ejector–diffuser system is employed to suck supersonic low-pressure and low-temperature flow into a high-pressure environment. A new design of a supersonic–supersonic ejector–diffuser was introduced to verify pressure control performance under different operating conditions and vacuum background pressure. A 1D analysis was used to predict the geometrical structure of an ejector–diffuser with a rectangular section based on the given operating conditions. Different numbers and types of nozzle plates were designed and installed on the ejector to study the realizability of avoiding or postponing the aerodynamic choking phenomenon in the mixing section. The effects of different geometrical parameters on the operating performance of the ejector–diffuser system were discussed in detail. Experimental investigation of the effects of different types of nozzle plates and the back pressures on the pressure control performance of the designed ejector–diffuser system were performed in a straight-flow wind tunnel. The results showed that the position, type and number of the nozzle plates have a significant impact on the beginning of the formation of aerodynamic choking. The geometry of the ejector and the operating conditions, especially the backpressure and inlet pressure of the ejecting stream, determined the entrainment ratio of the two supersonic streams. The experimental results showed that long nozzle-plate had a better performance in terms of maintaining pressure stability in the test section, while short a nozzle-plate had a better pressure matching performance and could maintain a higher entrainment ratio under high backpressure conditions.

Keywords: ejector; diffuser; turbulent mixing; pressure matching; nozzle array

check for updates

Citation: Xu, D.; Gu, Y.; Li, W.; Chen, J. Experimental Investigation of the Performance of a Novel Ejector–Diffuser System with Different Supersonic Nozzle Arrays. *Fluids* **2024**, *9*, 155. https://doi.org/10.3390/fluids9070155

Academic Editors: Markus Klein and Leonardo Santos de Brito Alves

Received: 26 May 2024
Revised: 23 June 2024
Accepted: 27 June 2024
Published: 2 July 2024

Copyright: © 2024 by the authors. Licensee MDPI, Basel, Switzerland. This article is an open access article distributed under the terms and conditions of the Creative Commons Attribution (CC BY) license (https://creativecommons.org/licenses/by/4.0/).

1. Introduction

Supersonic–supersonic ejectors are a type of fluid device in which two supersonic gas streams are mixed and compressed, and are widely used in aerospace science and technology [1,2]; high effective cooling systems, such as gas compression cooling systems [3–5]; jet refrigerator [4,6]; high-altitude wind tunnels [7–9]; and other energy systems dealing with exhaust gases and wind engineering [10–17]. Unlike traditional subsonic ejectors, the supersonic–supersonic ejector remains attractive and fascinating due to its high performance and compactness. In general, a good understanding of the shear interaction behavior between two supersonic streams, the interaction of shock waves [5,11], turbulent mixing [4,6], supersonic instability [15] and boundary and shear layers in the ejector [17] is both necessary and fundamental for designing effective ejector–diffuser systems. The major advantages of supersonic–supersonic ejectors are their structural simplicity and functional reliability when used for gas ejecting and supercharging. However, their main deficiency is also inevitable due to the fact that the two supersonic gas streams (the ejected stream

and the ejecting stream at the inlet of the mixing chamber) are mixed by only shear forces between these two streams, which means the static pressure difference between the ejected stream and the ejecting stream should not be too large to avoid aerodynamic choking [18]. For a supersonic–supersonic ejector, both the ejected stream and the ejecting stream are accelerated to supersonic flow through a convergent–divergent nozzle and the ejected stream will be over compressed. The kinetic energy of the ejecting stream converts into pressure energy in the limited mixing chamber and finally holds back the ejected flow due to the high backpressure. The static pressure ratio of the ejected stream to the ejecting stream at the occurrence of aerodynamic choking is called the limit pressure ratio. This should be considered especially during the design of the supersonic–supersonic ejector–diffuser system to improve its starting and supercharging performance.

It is extremely difficult to predict the flow structure and stream interactions inside the ejector–diffuser system because of the highly turbulent and supersonic mixing flow flooding in the mixing chamber. Prediction of the averaged flow in a supersonic ejector–diffuser has been based primarily on one-dimensional compressible-flow theory [19–21]. The classic theoretical and experimental research on supersonic ejector was performed by Eames et al. [22] using 1D models. Presently, 1D models are still used for the initial design of the ejector geometry based on what function the ejector is to be designed for. Traditionally, the main function of an ejector is to suck low-pressure gas to a relatively high-pressure environment. The flow behavior and the prediction of the shock waves are mainly investigated through CFD methods to optimize the ejector's geometrical structure, which show good agreement with experimental results, based on a large number of studies. Eames et al. [22] proposed a constant rate of momentum change (CRMC) approach to supersonic ejector design to minimize irreversibility and shock interactions. Yadav et al. [23,24] modified the CRMC models and theoretically developed a 1D dynamic gas method with a frictional effect for complete ejector design. Numerous reports indicated that the irreversible flow transition occurred at the entrance of the diffuser section and the nozzle exit position also had significant effects on the downstream. Lamberts et al. [25] numerically and experimentally investigated the aerodynamic choking phenomenon of the ejected stream in a supersonic ejector with an on/off design and under different operation conditions. Their result showed evidence of repeated Y-shock waves formed along the flow direction during the choking process under off design conditions. Wei et al. [26] numerically studied the transformation regularities of the flow structures of a multi-strut ejector (MSE) and they predicted multiple adjacent oblique shocks in a shock diamond matrix forming in the mixing chamber. They concluded that the wave loss, friction loss and mixing loss were the main factors that affected the evolution processes of multiple jets in the mixing chamber. Chong et al. [27] numerically analyzed the effects of the operation parameters and geometrical factors on an ejector's performance, and they verified that the static wall pressure along the flow direction remained constant under critical working conditions with different discharge pressures. Their experimental results also indicated that there existed an optimal nozzle exit position corresponding to a maximum entrainment ratio ($f = \dot{m}_2/\dot{m}_1$), but the critical value of the discharge pressure was almost independent of nozzle exit position. Rizzo et al. [28] proposed a new model based on the Spalart–Allmaras and RANS turbulent model to predict the transition mechanism from laminar to turbulent flow and they attested the accuracy of the model with two sets of experimental wind tunnel results.

Compared to CFD methods, direct observation and measurement of the flow parameters through experimental devices can provide much more intuitive and accurate comprehension of supersonic shear flow. Nevertheless, these processes have been much more complicated and uneconomical. Chong et al. [29] experimentally studied structural optimization and operating performance with natural gas and concluded that the optimal diameter ratio of the mixing tube to the primary nozzle throat was 1.6, the optimal ratio of length to diameter for the mixing tube was 4.0 and the optimal inclination angle of mixing chamber was 28°. Bouhanguel et al. [30] performed a flow visualization experiment on the shock structure, flow instabilities and mixing process in the supersonic ejector–diffuser

system using laser tomography techniques. Zhang et al. [31] studied the effect of internal surface roughness on ejector performance and they ascertained that the surficial friction force essentially degraded the working performance of the ejector–diffuser system. Zohbi et al. [32] investigated the effects of jet nozzle geometry and location on the performance of a supersonic ejector–diffuser system. The main conclusion they drew was that the geometric parameters should be changed to match optimal performance under a given set of operating conditions.

Based on the literature review, the geometrical parameters of an ejector and its operation parameters were the most important parameters in terms of the entrainment ratio of the ejecting stream to the ejected stream and the working performance of the ejector. Ejector–diffuser systems have different geometrical structures for different applications. The most discussed structure of ejectors is a circular cross-section which is not convenient for ground test facilities, such as wind tunnel experiments. Ejector–diffuser systems with a rectangular cross-section can provide a more uniform flow field and reduce the impact of boundary layers on the testing area compared with circular cross-section ejector–diffusers, which is advantageous in terms of obtain more accurate experimental data. Thus, it is necessary to figure out the supersonic flow behaviors and mechanisms inside ejector–diffuser systems with a rectangular cross-section.

In this paper, the geometrical parameters of an ejector–diffuser system with a rectangular section were initially calculated by using 1D design theory and the pressure performance of the ejector–diffuser system was tested in a wind tunnel. The main objective of this work was to design an ejector–diffuser system cooperating with a straight-flow wind tunnel and to create a stable rarefied supersonic flow in the test section. Our creative ideas were delaying the onset of the choking process and improving the pressure-boosting performance of the injector by designing different lengths and types of nozzle plates. The inlet surface area of the mixing chamber, partial parameters of the nozzle plate and the contraction ratio of the mixing chamber were determined during this calculation. Subsequently, the effects of different operation conditions and different types of nozzle plates on the pressure-matching performance of the designed ejector–diffuser system were experimentally studied in a straight-flow wind tunnel. The effects of the supersonic nozzle plate quantity and its geometrical dimensions were investigated with respect to the pressure distribution of the low-pressure chamber and the diffuser. The optimal operating conditions and the off design working boundary conditions of the ejector–diffuser system were clarified.

2. One-Dimensional Diffuser Model

As displayed in Figure 1, the proposed supersonic ejector was composed of the nozzle section, mixing chamber, secondary throat, subsonic diffuser and outlet section. The jet flow was accelerated by the designed supersonic nozzle plate. At the inlet of the mixing chamber, the total pressure $P_{t,2}$, static pressure P_2, static and total temperature T_2, $T_{t,2}$, ratio of specific heat γ_2, Mach number Ma_2, mass flow rate $\dot{m}_2$ and sectional area A_2 of the gas flow from the low-pressure chamber were given parameters. In general, the components of these two supersonic streams were different, which indicated that the difference in physical properties must be treated separately before and after the mixing process. In order to make the calculation process and formulas more concise and compact, we use velocity coefficients instead of Mach numbers. And the flow was treated as ideal compressible gas flow. The velocity coefficient was defined as the ratio of the gas velocity to the critical sound velocity, which was given by Equation (1).

$$\lambda = \frac{v}{a^*} = \frac{v(\gamma+1)}{2\gamma RT_t} \tag{1}$$

where the critical sound velocity $a^* = \sqrt{2\gamma RT_t/(\gamma+1)}$ was only determined by the total temperature, T_t. While the local sound velocity a depends on the local static temperature, T.

$$a = \sqrt{\gamma RT} \tag{2}$$

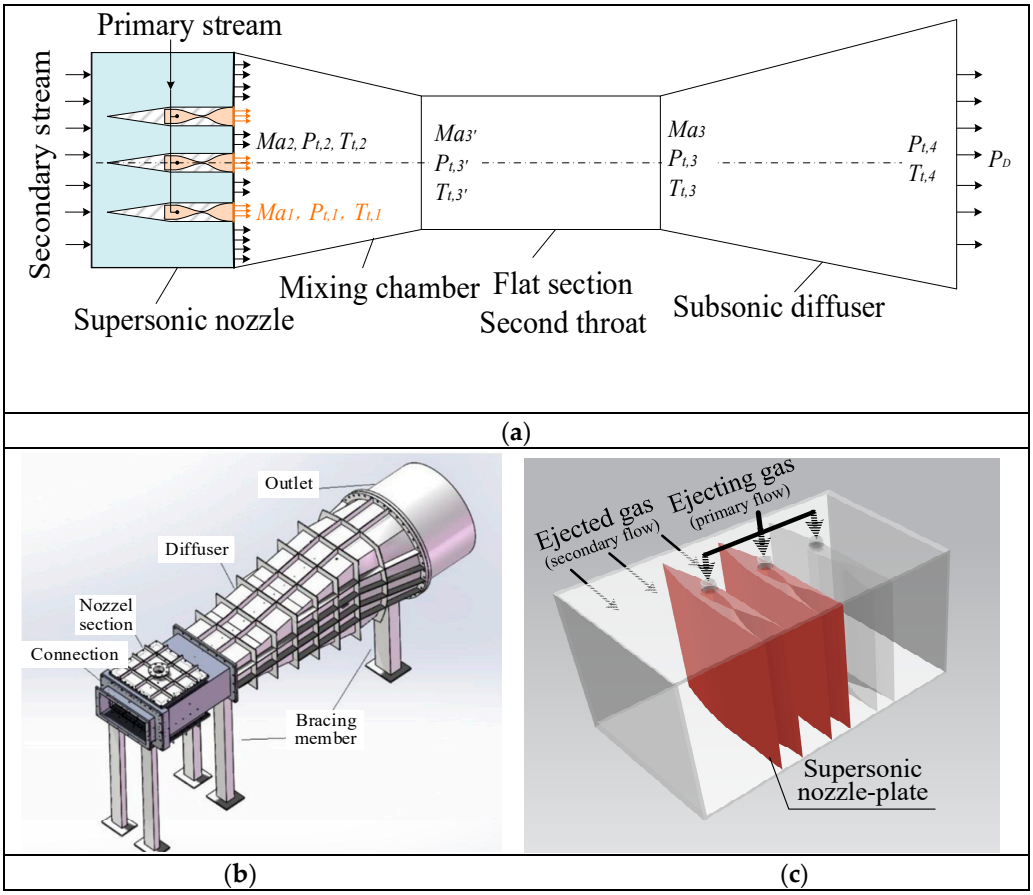


Figure 1. Schematic of (**a**) the flow arrangement of the 1D ejector–diffusor, (**b**) the three-dimensional model of the ejector–diffuser, (**c**) the 3D model and flow arrangement of the multi-nozzle section.

For adiabatic flow, which means constant total temperature in a supersonic nozzle, the static temperature T and the static pressure can be calculated from Equations (3) and (4).

$$\tau(\lambda,\gamma) = \frac{T}{T_t} = 1 - \lambda^2 \frac{\gamma-1}{\gamma+1} \tag{3}$$

$$\pi(\lambda,\gamma) = \frac{P}{P_t} = \left(1 - \lambda^2 \frac{\gamma-1}{\gamma+1}\right)^{\frac{\gamma}{\gamma-1}} \tag{4}$$

By introducing the definition of Mach number, $Ma = v/a$, the relationship between the velocity coefficient and the Mach number can be given by Equation (5).

$$\lambda \sqrt{\frac{2\gamma}{\gamma+1} RT_t} = Ma\sqrt{\gamma RT} \tag{5}$$

By substituting Equation (3) into Equation (5), the Mach number and the velocity coefficient can be written as

$$Ma = \sqrt{\frac{2\lambda^2}{(\gamma+1)\left(1-\lambda^2\frac{\gamma-1}{\gamma+1}\right)}} \tag{6}$$

$$\lambda = \sqrt{\frac{(\gamma+1)Ma^2}{2\left(1+\frac{\gamma-1}{2}Ma^2\right)}} \tag{7}$$

Assuming adiabatic isentropic flow was satisfied in the supersonic ejector nozzle, the outlet Mach number of the supersonic ejector nozzle can be predicted by Equation (8).

$$Ma_1 = \sqrt{\frac{2}{\gamma_1 - 1}\left[\left(\frac{P_{t,1}}{P_1}\right)^{\frac{\gamma_1 - 1}{\gamma_1}} - 1\right]} \tag{8}$$

where $P_{t,1}$ and P_1 arere the total pressure and static pressure of the ejecting flow, respectively. The two supersonic streams, with Mach numbers Ma_1 and Ma_2, exchanged momentum and energy in the flat following section where the side mini-nozzles were installed to prevent the growth of the velocity boundary layer.

Assuming these two supersonic streams were fully mixed to a homogeneous flow in the mixing chamber, the physical properties of the mixed flow can be evaluated.

$$\frac{c_{P_{3'}}}{c_{P_1}} = \frac{1 + f\xi}{1 + f} \tag{9}$$

$$R_{3'} = \frac{R_1 + fR_2}{1 + f} \tag{10}$$

$$\gamma_{3'} = \frac{1 + f\xi}{\gamma_2/\gamma_1 + f\xi}\gamma_2 \tag{11}$$

where f is the ratio of the mass flow rate (the entrainment ratio) $\dot{m}_2/\dot{m}_1$, ξ is the ratio of the specific heat $c_{p,1}/c_{p,2}$ and R is the gas constant number.

Then, the thermodynamic parameters of the mixed downstream can be derived by applying the mass conversation and energy conversation law at the mixing section

$$\dot{m}_{3'} = \dot{m}_1 + \dot{m}_2 = (1 + f)\dot{m}_1 \tag{12}$$

$$\dot{m}_{3'} c_{P_{3'}} T_{t,3'} = \dot{m}_1 c_{P_1} T_{t,1} + \dot{m}_2 c_{P_2} T_{t,2} \tag{13}$$

Substituting Equations (9)–(11) into Equations (12) and (13), the total temperature and static pressure were obtained.

$$\frac{T_{t,3'}}{T_{t,1}} = \frac{1 + f\xi\theta}{1 + f\xi} \tag{14}$$

$$\frac{P_{3'}}{P_2} = \frac{p_1}{p_2}\frac{\pi_{3'}\Gamma_1 q_1}{\pi_1 \Gamma_3 q_3}\frac{A_1 + A_2}{A_1}\sqrt{\frac{1 + f\xi\theta}{1 + f\xi}} \tag{15}$$

where θ is the ratio of total temperature $T_{t,2}/T_{t,1}$. The parameters of Γ and q are functions of local physical properties, written as

$$\Gamma(\gamma, R) = \left(\frac{2}{\gamma + 1}\right)^{\frac{\gamma + 1}{2(\gamma - 1)}}\left(\frac{\gamma}{R}\right)^{\frac{1}{2}} \tag{16}$$

$$q(\lambda, \gamma) = \frac{\rho u}{\rho^* u^*} = \lambda\left(\frac{\gamma + 1}{2}\right)^{\frac{1}{\gamma - 1}}\left(1 - \lambda^2\frac{\gamma - 1}{\gamma + 1}\right)^{\frac{1}{\gamma - 1}} \tag{17}$$

Now the momentum equation of the mixing section is given by Equation (18).

$$\dot{m}_{3'} V_{3'} - (m_1 V_1 + m_2 V_2) = (P_1 A_1 + P_2 A_2) - P_{3'} A_{3'} + \int_{wall} P(x)dx \tag{18}$$

where the $P(x)$ term is thinner wall pressure distribution along the gas flow in the mixing section, thus the integral term $\int_{wall} P(x)dx$ represents the net frictional force acting on the fluid. This force accounts for the interaction and momentum loss due to the mixing process

which has a strong correlation with the geometrical parameter of the mixing section. As proposed in ref. [22], a reasonable and simplified estimation of the wall pressure distributed linearly along the flow direction was used.

$$\int_{wall} P(x)dx = -\frac{P_1 + P_{3'}}{2}(A_1 + A_2 - A_{3'}) \tag{19}$$

Substituting Equation (19) into Equation (18) and combining this with Equations (5), (9)–(11), (14) and (15), the velocity coefficient $\lambda_{3'}$ can be derived as

$$\begin{aligned} &\lambda_{3'}(1+f)\sqrt{\tfrac{1+f\bar{\xi}\theta}{1+f\bar{\xi}}}\sqrt{\tfrac{2\gamma_{3'}R_{3'}}{\gamma_{3'}+1}} - \lambda_1\sqrt{\tfrac{2\gamma_1 R_1}{\gamma_1+1}} - \lambda_2\sqrt{\tfrac{2\lambda_2 R_2}{\lambda_2+1}} = \\ &\Psi_1\sqrt{\tfrac{2\gamma_1 R_1}{\gamma_1+1}}\left(\tfrac{1+\beta}{2\alpha n} + \tfrac{n-1}{n}\right) - \Psi_{3'}\sqrt{\tfrac{2\gamma_{3'}R_{3'}}{\gamma_{3'}+1}}(1+f)\sqrt{\tfrac{1+f\bar{\xi}\theta}{1+f\bar{\xi}}}\tfrac{1+\beta}{2\beta} \end{aligned} \tag{20}$$

where α and β are the ratio of the area at the inlet and outlet of the mixing sections $\alpha = A_1/(A_1 + A_2)$ and $\beta = A_3/(A_1 + A_2)$, respectively. The factor n is the pressure ratio of the ejecting to the ejected gas $n = P_1/P_2$. $\Psi(\lambda, \gamma)$ is the combined aerodynamic function, defined as

$$\Psi(\lambda,\gamma) = \frac{\pi}{\Gamma q}\left(\frac{2\gamma}{1+\gamma}R\right)^{-1/2} = \lambda^{-1}\left(1 - \lambda^2\frac{\gamma-1}{\gamma+1}\right)\frac{\gamma+1}{2\gamma} \tag{21}$$

Based on Equation (6), the Mach number at Section 3, $Ma_{3'}$, can be expressed as

$$Ma_{3'} = \sqrt{\frac{2{\lambda_{3'}}^2}{(\gamma_{3'}+1)\left(1 - {\lambda_3}^2\frac{\gamma_{3'}-1}{\gamma_{3'}+1}\right)}} \tag{22}$$

It was reasonable to assume that the mixed supersonic flow transformed into subsonic flow after crossing a normal shock in the flat section. Then, the Mach number and pressure ratio at Section 3 can be predicted as

$$Ma_3 = \sqrt{\frac{\frac{2}{\gamma_{3'}-1} + Ma_{3'}^2}{\frac{2\gamma_{3'}Ma_{3'}^2}{\gamma_{3'}-1} - 1}} \tag{23}$$

$$\frac{P_3}{P_{3'}} = \frac{1 + \gamma_{3'}Ma_{3'}^2}{1 + \gamma_{3'}Ma_3^2} \tag{24}$$

Finally, the ratio of total pressure is given by Equation (25). The pressure ratio of the ejector can be expressed as $P_{t,4}/P_{t,2}$ according to Equations (15) and (24), which indicate the efficiency of the multi-nozzle ejector.

$$\frac{P_{t,4}}{P_{t,3}} = \left(1 + \frac{\gamma_3 - 1}{2}Ma_3^2\right)^{\frac{\gamma_3}{\gamma_3-1}} \tag{25}$$

3. Experimental Setup

As shown in Figure 2, two gas reservoirs with pressure limits of 1 MPa and 2 MPa were employed as the source supply for the ejected stream and ejecting stream, respectively. The initial source gas parameters for the nozzle plates are listed in Table 1 and the parameters of the ejected gas are listed in Table 2. The source injecting gas was air and the ejected gas was a homogenic mixture of oxygen, chlorine, iodine vapor and helium gas. Both gas reservoirs were connected to a compressor, which was used to maintain the source gas pressure to ensure efficient gas supply to the tunnel and nozzles. The ejected stream was accelerated to Ma = 2.4 by a supersonic nozzle through a straight-flow wind tunnel. The inlet pressure was controlled by a pressure regulator and the mass flow rate was measured

by a mass flow meter. The designed ejector–diffuser system consisted of four sections: the supersonic nozzle plate section, mixing chamber, second throat (the flat section) and the subsonic diffuser. Figure 1b shows the 3D structure of the ejector–diffuser system, which was connected to the supersonic diffuser of the straight flow wind tunnel to obtain the supersonic incoming flow. As shown in Figure 1c, the supersonic nozzle plate was designed to obtain a supersonic flow of Ma = 4.5 based on the source gas parameter. The number and the length of the nozzle plates can be adjusted according to different experiment demands. The experimental setup is schematically shown in Figure 2, with five static wall pressure apertures located on the supersonic diffuser and twenty-six apertures located on the subsonic diffuser. Before the experiment, the straight-flow wind tunnel was pre-started and allowed to reach a stable state. Pressure data were recorded using a pressure scanning valve with an accuracy of ±0.05%. The ejecting stream was accelerated to supersonic flow at the outlet surface of the nozzle plate and mixed with supersonic flow from the wind tunnel in a mixing chamber, as shown in Figure 1c. The velocity of the mixed stream decreased and the pressure energy increased in the converging section. In the following flat section and the diffuser section, the pressure of the fully mixed stream continued to rise until the flow turned into subsonic flow and finally was collected by the vacuum reservoir. Experiments on different types of nozzle plates and backpressures were conducted to examine the pressure-matching performance of the designed ejector–diffuser system.

Table 1. Inlet air (functioning as a source gas) parameters of the ejecting stream.

Parameters	Value	Unit
Ma_1	4.5	-
$T_{t,1}$	300	K
$P_{t,1}$	0.5~2.0	MPa
γ_1	1.4	-
R_1	287	J kg^{-1} K^{-1}

Table 2. Input operating condition of the ejected mixture stream in the designed ejector–diffuser.

Parameters	Value	Unit
Ma_2	2.4	-
$T_{t,2}$	600	K
$P_{t,2}$	0.2~100	kPa
γ_2	1.5	-
R_2	849	J kg^{-1} K^{-1}

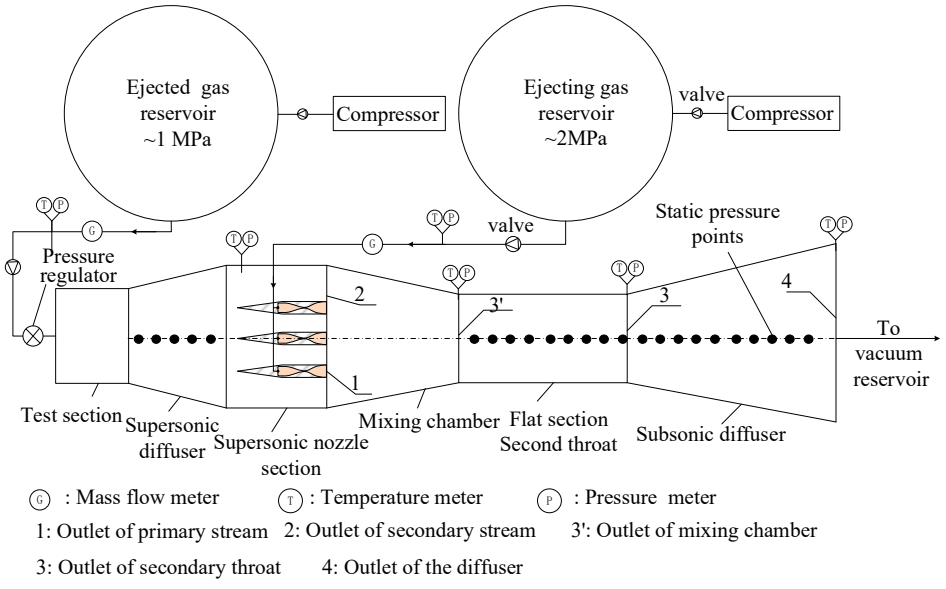


Figure 2. Experimental setup of designed ejector–diffuser.

4. Results and Discussion

4.1. Design and Analysis of Ejector–Diffuser System

4.1.1. Performance Parameters vs. Velocity Coefficient

Figure 3 presents the relationship between the relevant velocity coefficient and the concerned parameters of the designed ejector regarding different mixing flow conditions. As shown in Figure 3a, the outlet velocity coefficient of the mixing section increased with increasing contraction ratios, as the kinetic energy was converted into pressure potential energy when the mixed supersonic air stream flowed through the contraction section. In the mixing section, the total pressure of the mixed air flow increased with an increasing velocity coefficient but decreased when the velocity coefficient of the mixed air flow was larger than 1.7, as indicated in Figure 3b. There existed a minimum value of contraction ratio of $A_{3'}/(A_1 + A_2)$, a maximum pressure ratio value of $P_{t,3'}/P_{t,2}$ and $P_{t,4}/P_{t,2}$ with the increasing velocity coefficient λ_3. Meanwhile, the pressure ratio $P_{t,3}/P_{t,3'}$ decreased with the increasing velocity coefficient λ_3. For a mixing section with a large contraction ratio $A_{3'}/(A_1 + A_2) > 0.55$, the outlet total pressure $P_{t,4}$ would drop rapidly as shown in Figure 3d, leading to the performance degradation of the ejector and a failure to maintain high vacuum conditions in the test chamber. Thus, the pressure ratio of the ejector was the most important parameter in terms of evaluating the performance of the designed diffuser system.

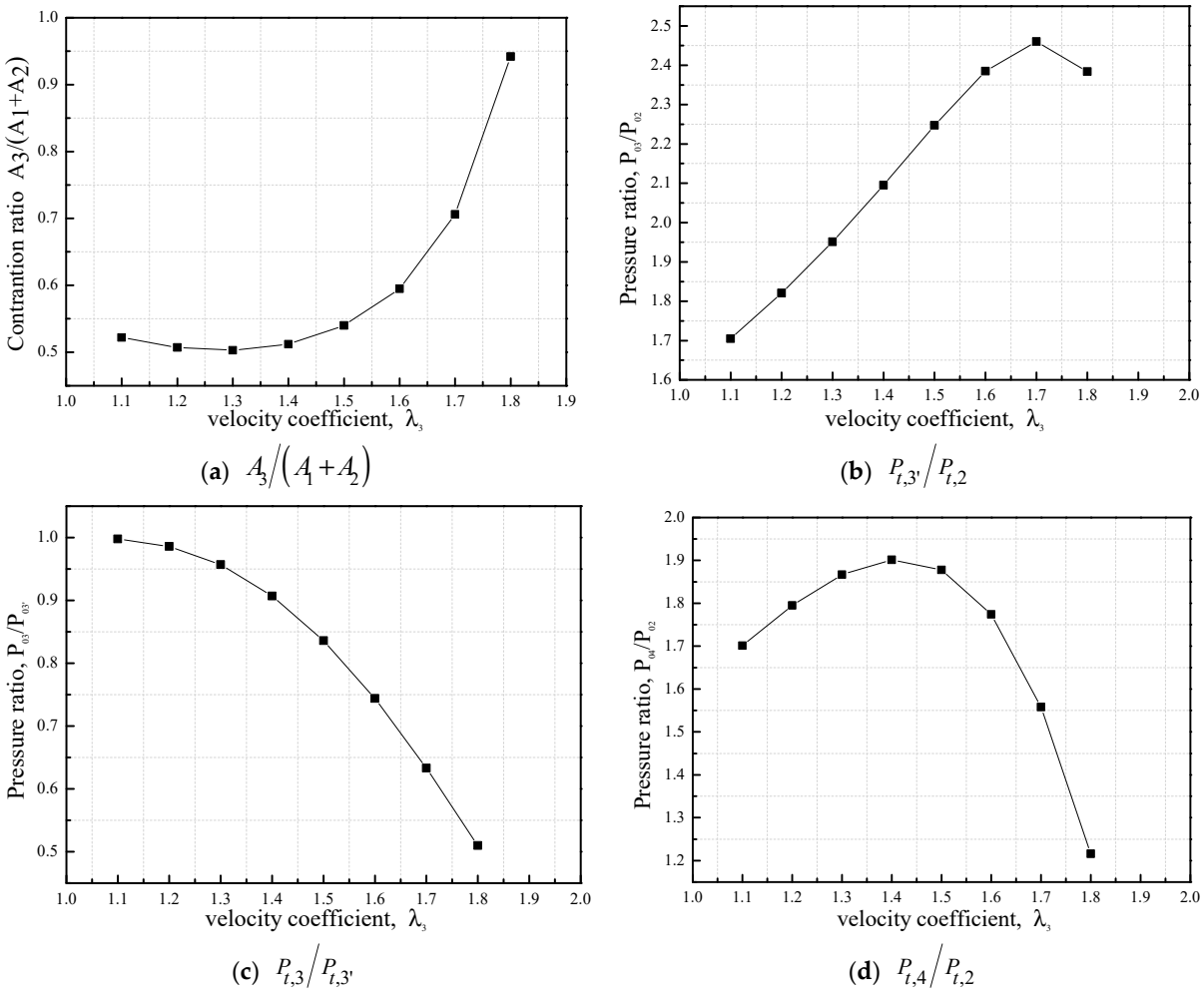


Figure 3. Effect of velocity coefficient on (**a**) the contraction ratio of the mixing section, (**b**) the ratio of total pressure $P_{t,3'}/P_{t,2}$ in the mixing section, (**c**) the pressure drop factor of the normal shock in the flat section, (**d**) the pressure ratio of the supersonic ejector after a normal shock.

As defined in Equation (1), the velocity coefficient was a function of the total temperature T_t and the specific heat ratio $\gamma = c_p/c_v$. During the design and calculation process of the mixing section, the velocity coefficient of the mixed supersonic streams should achieve its optimal value at the outlet section by considering the comprehensive effects of the ratio of mass flow rate and the total inlet temperature of the ejecting steam. Meanwhile, the contraction ratio and the geometry parameters of the ejecting branches also affected the mixing process of the two supersonic streams. The most important objectives were to obtain a homogeneous supersonic flow at the outlet surface of the mixing section and to maintain a low vacuum state in the low-pressure chamber in front of the diffuser.

4.1.2. Effect of Mach Number

For a supersonic–supersonic ejector, both the ejecting stream and the ejected stream exhibited supersonic flows in the mixing section. The pressure, Mach number and temperature of the ejected stream are given in Tables 1 and 2, and efforts were targeted on determining the nozzle and flow parameters of the ejecting flow. For fixed nozzles and the inlet pressure of the ejecting stream (primary flow), the performance of the diffuser–ejector system was depended on the ejected stream (secondary flow) parameters. As shown in Figure 4, the stagnation pressure ratio of the diffuser increased initially with the velocity coefficient and decreased afterwards when the velocity coefficient λ_3 was larger than 1.4. When the Mach number of the secondary flow increased from 1.8 to 2.4, the stagnation pressure ratio decreased from 3.32 to 1.90 at velocity coefficient $\lambda_3 = 1.4$. The pressure loss of the mixed stream was mainly caused by the decreased static pressure of the secondary flow with increasing Mach number, which resulted in further expansion and deceleration of the primary flow. The stagnation pressure ratio reflected the pressure recovery performance of the diffuser, which was the primary demand of the connected device. It should be noted that the velocity-matching performance could also be achieved by adjusting the flow parameters of the ejecting stream to a higher velocity coefficient to obtain a higher stagnation pressure ratio. Therefore, the mass flow rate and the static pressure of the ejecting stream were both designed to be adjustable to meet the variable operating conditions of the secondary flow.

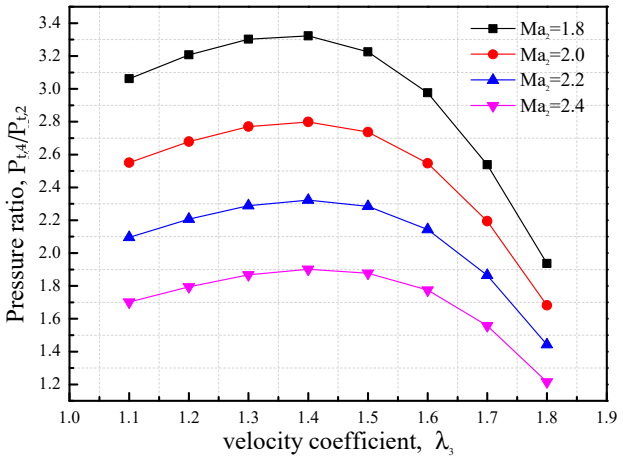


Figure 4. Effect of Mach number of the ejected stream on the diffuser compression ratio.

Figure 5 shows the stagnation pressure ratio of the diffuser under different Mach numbers of the primary stream, ranging from 4.2~5.0. The stagnation pressure ratio of the diffuser also initially increased with the velocity coefficient and then decreased sharply. Additionally, the stagnation pressure ratio increased with the increasing Mach number of the ejecting stream since the inlet pressure increased with the increasing Mach number of the ejecting stream, resulting in the pressure rise in the mixed flow. For both Figures 4 and 5, the optimal value of the velocity coefficient for the mixed stream was ~1.4 for the diffuser

based on the given parameters, and the stagnation pressure ratio of the diffuser was more sensitive to the Mach number of the ejected stream than the primary flow.

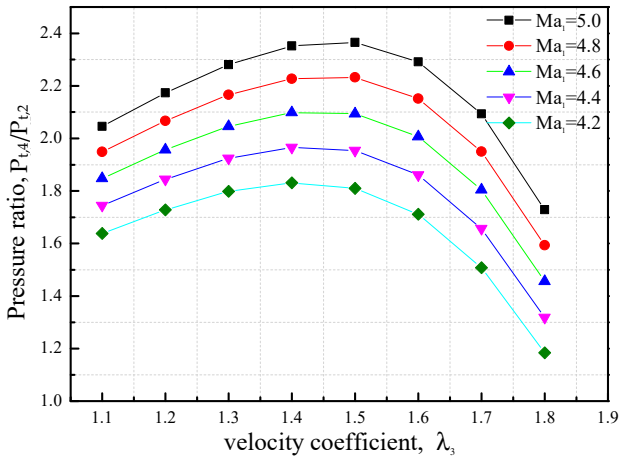


Figure 5. Effect of Mach number of the ejecting stream on the diffuser compression ratio.

4.1.3. Effect of Mass Flow Rate

Figure 6 demonstrates diffuser performance with different mass flow ratios of the ejected stream to the ejecting stream, $f = \dot{m}_2/\dot{m}_1$ ranging from 0.1 to 0.2. The result shows that the stagnation pressure ratio of the diffuser increased with the decreasing mass flow ratio. For a given nozzle in the ejector, the mass flow rate of the ejecting stream was directly influenced by the total pressure when supersonic flow was established throughout the nozzle plates. However, an excessive pressure difference between the primary flow and the secondary flow could cause aerodynamic choking in the mixing chamber. In severe cases, the ejected stream could be throttled by the expansion of the primary flow, which would make the ejector operate ineffectively and even reach an off state. With the increasing ratio of mass flow rate, the pressure ratio of the mixed flow $P_{t,4}/P_{t,2}$ decreased due to the decrement of the partial pressure of the primary stream in the flow duct. Under these circumstances, the cross-sectional area ratio of the nozzle needed to be increased for the primary flow to expand the scope of the mass flow rate and the pressure operating range of the primary flow nozzle. Additionally, the total energy of the mixed flow decreased due to the decrement of the primary flow rate, resulting in a larger contraction ratio $A_{3'}/(A_1 + A_2)$ of the mixing chamber and a smaller velocity coefficient λ_3.

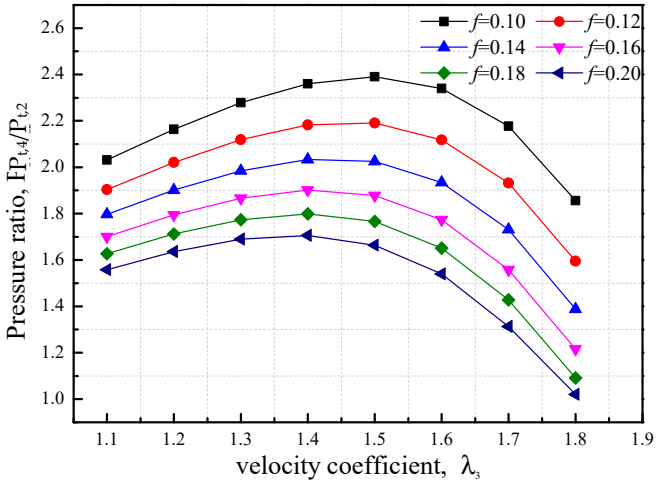


Figure 6. Effect of mass flow ratio of the ejected stream to the ejecting stream on the diffuser compression ratio.

4.1.4. Effect of Static Pressure

Figure 7 showed the stagnation pressure ratio results of the ejector under different static pressure ratios (P_1/P_2) of the ejected stream to the ejecting stream. The static pressure was specified at the inlet of the mixing chamber. The results indicated that the stagnation pressure ratio $P_{t,4}/P_{t,2}$ initially increased with the velocity coefficient λ_3 and decreased when the velocity coefficient was larger than 1.5. For low static pressure conditions ($P_1/P_2 < 0.6$), the stagnation pressure ratio was smaller than 1.5, which may have indicated a stalled state of the supersonic–supersonic ejector and diffuser system. Conversely, for high static pressure conditions ($P_1/P_2 > 1.4$), the ejected flow was excessively compressed by the ejecting flow, increasing the risk of aerodynamic choking and over-damning of the ejecting flow. Therefore, it can be inferred that the static pressure ratio should be close to unity to avoid aerodynamic choking and the dead-start of the supersonic–supersonic ejector and diffuser system. The mass flow ratio can be adjusted by modifying the geometric parameters of the ejecting nozzle. Based on these conditions, the recommend range for the static pressure ratio was from 0.8 to 1.2.

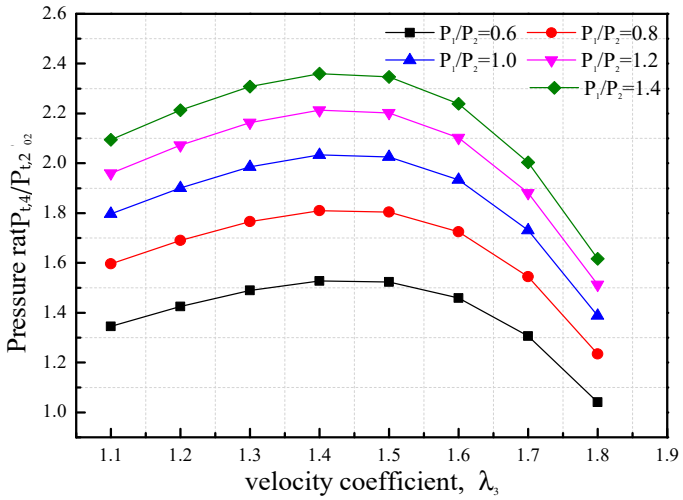


Figure 7. Effect of static pressure ratio of the ejecting stream to the ejected stream on the diffuser compression ratio.

4.2. Static Wall Pressure of Supersonic Diffuser

Experimental investigation of the pressure control performance of the designed ejector–diffuser system in a straight-flow wind tunnel was performed. The five measuring points are marked in Figure 2 and the static wall pressures were recorded. Firstly, the ejector–diffuser system was not started (with no supersonic nozzles installed) and only worked as a flow channel for the ejected stream. The ambient pressure at the outlet of the ejector–diffuser was regulated by the vacuum reservoir with an adjustable pressure range from 0.1 P_D to 6.0 P_D. Figure 8 shows the results of the dimensionless pressure distribution of the supersonic diffuser when the connected ejector–diffuser system was not started. The results show that the pressure changed stably along the flow direction with the dimensionless pressure P_b/P_D ranging from 0.2 to 0.8, which indicates that the flow inside the tunnel was a fully developed supersonic stream. The wall pressure increased sharply when the dimensionless pressure ratio, P_b/P_D, came to be greater than 1.1. This indicated a flow deceleration and increment of potential energy. Additionally, the occurrence of a shock wave near the tunnel wall also increased the wall pressure and decreased the flow velocity.

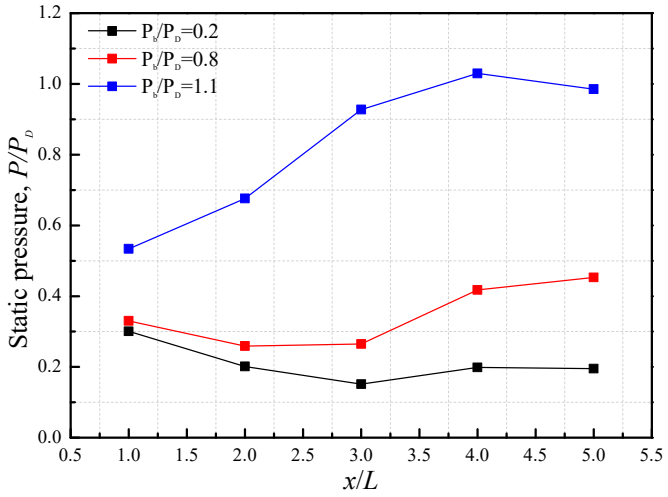


Figure 8. Pressure distribution of the supersonic diffuser under different backpressures, while the ejector–diffuser has not been started. The supersonic diffuser was in front of the nozzle section.

Figure 9 presents the static wall pressure distribution of the supersonic diffuser with different ejector–diffuser systems. Different types of supersonic nozzle plates were clamped onto the nozzle section. As displayed in Figure 1c, all supersonic nozzles were embedded in the wedge plate to reduce flow resistance of the ejected stream. The gas source of these nozzles was supplied and supercharged by a compressor to ensure sufficient inlet pressure and supersonic flow at the outlet of nozzles. Figure 9a shows the results of the static wall pressure when three long nozzle plates were used in the ejector–diffuser system. The results show that a low pressure and vacuum environment ($P_b/P_D < 0.4$) can be maintained in the supersonic diffuser chamber when the dimensionless pressure P_b/P_D of the vacuum reservoir was below 2.0. In contrast, the static pressure increased obviously along the flow direction when the dimensionless pressure P_b/P_D increased to 4.5, which indicated that the flow condition in the supersonic diffuser was changed by the high backpressure of the ejector–diffuser system. It should be noted that high backpressure could decelerate the ejected stream and result in choking the flow in the supersonic nozzle section. Additionally, the flow structure and shock wave in the supersonic diffuser can be affected by the nozzle section and even the mixing process in the mixing chamber due to the hyperbolic characteristics of the supersonic flow. Figure 9b displays the static wall pressure results of the supersonic diffuser when backpressure P_b/P_D ranged from 3.5 to 4.5. Compared with the conditions of no nozzle plate shown in Figure 9d, a stable and smooth pressure distribution can be maintained in the supersonic diffuser with the installation of long nozzle plates in the nozzle section when the backpressure of the ejector–diffuser system is lower than two times the characteristic pressure, $2P_D$. Compared with Figure 9a,b, the pressure results of the three short nozzle plates seemed to provide better performance under high-backpressure conditions. Even though the backpressure P_b/P_D increased to 5.2, the static wall pressure was still smaller than P_D. The static wall pressure increased with the increasing backpressure; while obviously remaining lower than that with long nozzle plates in Figure 9a,b. This indicates that the ejector–diffuser system with three short nozzle plates had less effect on the upstream and showed a better capability to maintain supersonic flow conditions and a stable vacuum environment in the supersonic diffuser. Based on these experimental tests, it can be found that the number and length of the nozzle plates had a significant influence on the static wall pressure distribution and the supersonic flow conditions in the supersonic diffuser, which determined the working conditions of the supersonic diffuser.

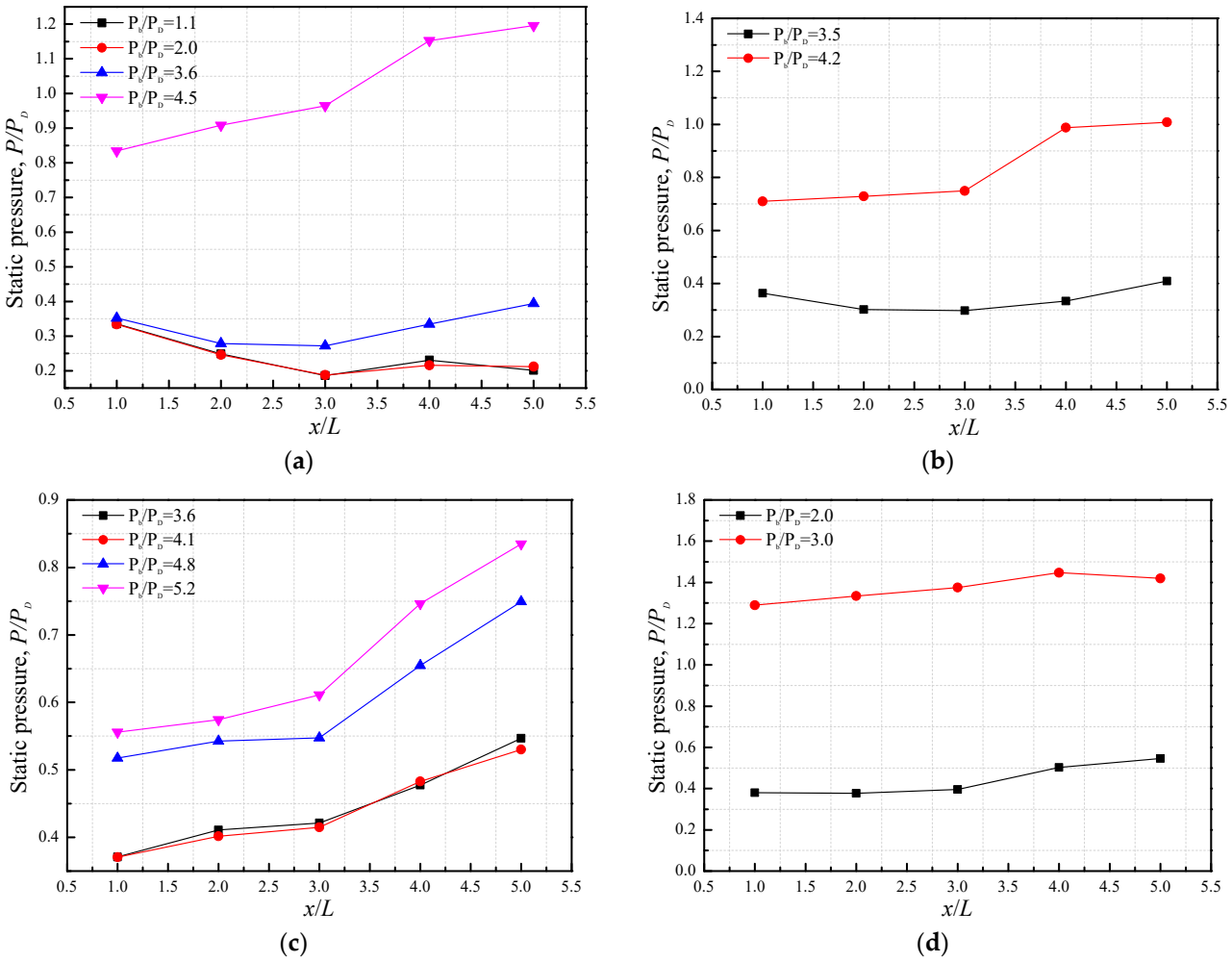


Figure 9. The ejector–diffuser performance and effects on the wall pressure stability of the supersonic diffuser with different types of supersonic nozzles. The nozzle section connected with (**a**) three long supersonic nozzle plates; (**b**) four long supersonic nozzle plates; (**c**) three short supersonic nozzle plates, and (**d**) no nozzle plates but with boundary layer bleeding.

4.3. Performance of Ejector–Diffuser

4.3.1. Pressure Controlling Performance in Wind Tunnel Test

Figure 10 displayed the static wall pressure measured from the flat section to the subsonic diffuser, as marked in Figure 1a. For the ejector–diffuser system with three long nozzle plates, the static wall pressure increased with the increasing back pressure P_b / P_D, ranging from 1.1 to 4.5, as shown in Figure 10a,b. Based on the results in Figure 9a,b, it can be concluded that the ejector–diffuser system with long nozzle plates worked efficiently when the back pressure was lower than 3.5~3.6 P_D, indicating that the pressure disturbance at the outlet of the diffuser cannot affect the upstream in the supersonic section. This meant that the designed ejector–diffuser system can boost the low-pressure gas (0.2~0.4 P_D) in the test section and supersonic section to a high-pressure state of approximately 3.5~3.6 times of the designed back pressure, P_D, which made it possible to exhaust the low vacuum and pressure gas of the secondary flow to atmosphere with moch less energy consumption. As seen in Figure 10c, the ejector–diffuser system with three short nozzle plates had a better ability of stabilizing the pressure in the supersonic diffuser and maintaining a stable vacuum environment. By using the short nozzle plates, the back pressure of the ejector–diffuser can be improved to 4.1 P_D, nearly without any disturbance on the test and supersonic section. However, the static wall pressure increased from 0.2 P_D to 0.6 P_D when the back pressure increased to higher than 5.2 P_D, which indicated that the supersonic diffuser and

the test section cannot provide the desired experimental operating conditions. As analyzed in Section 4.1, mass flow rate can be improved by increasing the inlet stagnation pressure of the ejecting flow through increasing the back pressure. However, too high pressure of the ejecting stream can result in aerodynamic choking. Thus, the operation of the working parameters must be based on the actual demand and experimental conditions.

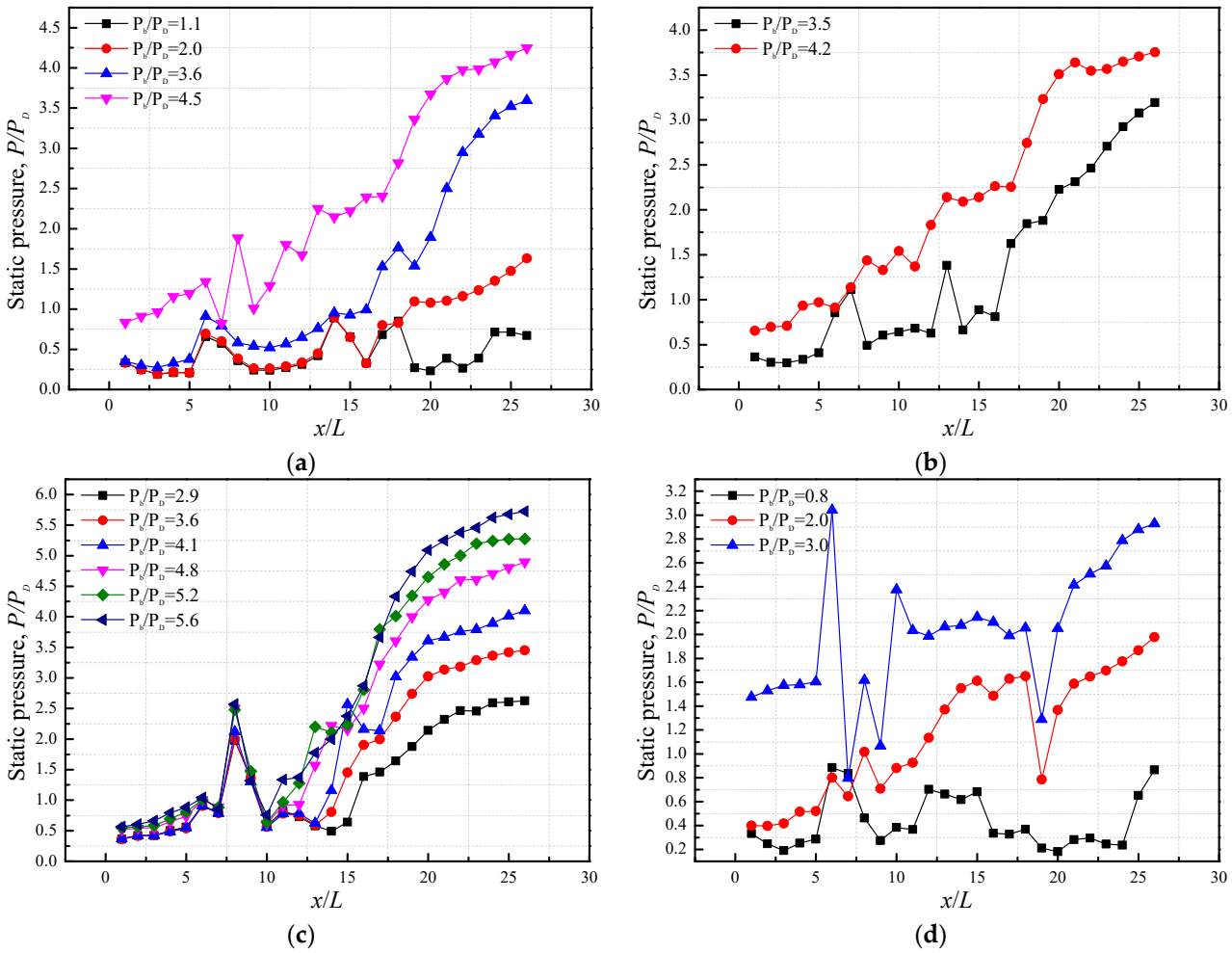


Figure 10. Static wall pressure distributions of the secondary throat and the subsonic diffuser of the ejector–diffuser system with different types of supersonic nozzles. The nozzle section was installed with (**a**) three long supersonic nozzle plates; (**b**) four long supersonic nozzle plates; (**c**) three short supersonic nozzle plates, and (**d**) no nozzle plates but with boundary layer bleeding.

4.3.2. Power Enhancement for COIL Laser

As shown in Figure 11a, the instantaneous pressure in the test section was displayed to validate the pressure controlling performance of the designed ejector–diffuser system. The experimental COIL laser setup was started first without enabling the ejector–diffuser system. The pressure reached a steady value of 0.36 P/P_D after 10 s. Subsequently, the ejector–diffuser system was started, and the pressure decreased rapidly and a lower pressure environment was achieved in the test section. The result showed that the minimum pressure in the test section can be controlled stably as low as 0.19 P/P_D, which improved the output power of the COIL laser by approximately 14.1% compared to the disabled ejector–diffuser condition. The experimental results showed that the ejector–diffuser system had a remarkable effect on maintaining a high-vacuum environment and improving the output power intensity of the COIL laser test rig.

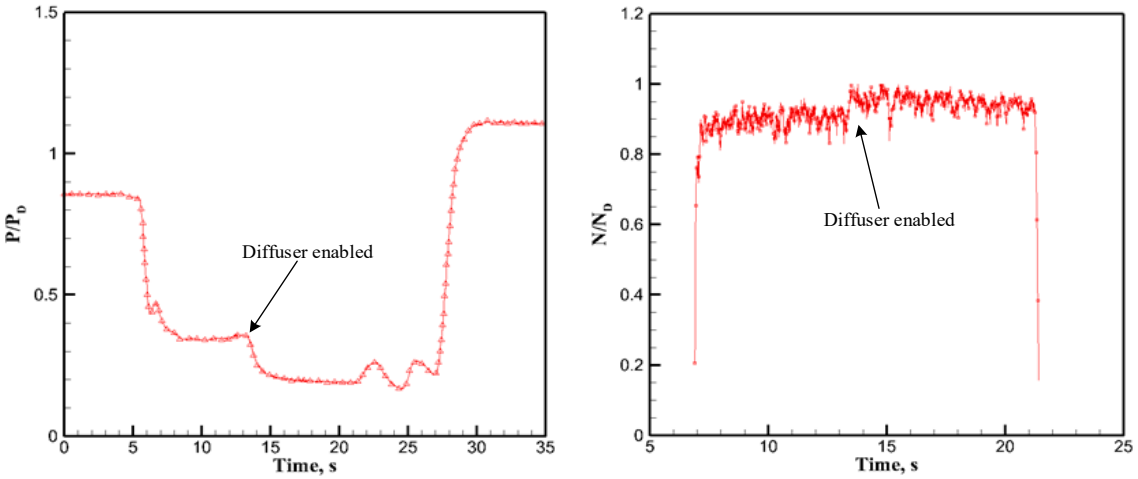


Figure 11. Experimental results of (**a**) the pressure control performance of the ejector–diffuser system, (**b**) the output power performance of a COIL laser test rig with the ejector–diffuser system started.

5. Conclusions

The present work presented a complete design analysis for a 1D ejector–diffuser system with a rectangular section under given operating conditions. A method to improving the operating performance by replacing nozzle sections with different types and numbers of nozzle plates was proposed. Experimental investigation on effects of different types of nozzle plates and the backpressures on the pressure boosting performance of the designed ejector–diffuser system were tested in a straight-flow wind tunnel. The following conclusions have been drawn:

(1) For given inlet gas parameters, the initial cross-section area of the supersonic–supersonic ejector–diffuser can be determined through 1D analysis. It was found that the optimal contraction ratio of the mixing chamber can be predicted by the designed pressure ratio and mass flow ratio.

(2) The aerodynamic choking phenomenon occurs when the inlet pressure of the ejecting stream reaches a critical value, resulting in the high-frequency vibration of the ejector system. Therefore, the off-designed operating condition should be clarified and avoided.

(3) The position, type and number of nozzle plates have a significant influence on the pressure-boosting ability. For an ejector–diffuser system with three long nozzle plates, the outlet pressure of the ejector can be boosted to a maximum value of 4.5 P_D, while an ejector–diffuser system with three short nozzle plates has a better ability in terms of stabilizing pressure, and the outlet pressure can be improved to 4.1 P_D~5.2 P_D.

(4) The designed supersonic–supersonic ejector–diffuser system has a wide range of working conditions and is economically viable. Different operating conditions can be realized by changing the number and type of nozzle plates. The experimental results show that long nozzle plates exhibit better performance in terms of maintaining pressure stability in the test section while short nozzle plates have a better pressure-matching performance and entrainment ratio under high-backpressure conditions.

(5) The boundary layer and the shock interaction can be easily controlled by adjusting the position of the nozzle plate in a supersonic–supersonic ejector with a rectangular section compared with a round ejector. The boundary layer can be destroyed by setting the supersonic nozzle plate near the wall region.

Author Contributions: D.X.: conceptualization, methodology, validation and experimentation; Y.G.: writing—review and editing, conceptualization and supervision; W.L.: writing—review and editing;

J.C.: methodology, experimentation, writing—original draft and writing—review and editing. All authors have read and agreed to the published version of the manuscript.

Funding: This research was funded by the National Natural Science Foundation of China, grant number 52106215.

Data Availability Statement: The data presented in this study are available on request from the corresponding author.

Conflicts of Interest: The authors declare no conflict of interest.

Nomenclature

A	Sectional area, m^2
c_p	Specific heat, J kg^{-1} K^{-1}
a	Sound velocity, m s^{-1}
a^*	Critical sound velocity, m s^{-1}
v	Gas velocity, m s^{-1}
f	Entrainment ratio, $\dot{m}_2/\dot{m}_1$
Ma	Mach number
n	Pressure ratio, $n = p_1/p_2$
$\dot{m}_2$	Mass flow rate, kg s^{-1}
P	Static pressure, kPa
P_t	Total pressure, kPa
R	Global gas constant number
T_t	Total temperature, K
T	Static temperature, K
Greek Symbols	
α	Ratio of area, $\alpha = A_1/(A_1 + A_2)$
β	Ratio of area, $\beta = A_3/(A_1 + A_2)$
λ	Velocity coefficient, $\lambda = v/a^*$
γ	Ratio of specific heat, $\gamma = c_p/c_v$
ξ	Ratio of specific heat, $c_{p,1}/c_{p,2}$
θ	Ratio of total temperature, $T_{t,2}/T_{t,1}$
Subscripts	
0	Stagnation parameter
1	Outlet of nozzle-plates
2	Outlet of nozzle section
3′	Outlet of mixing chamber
3	Outlet of flat section
4	Outlet of subsonic diffuser

References

1. Zhang, J.; Geng, J.; Yang, S.; Cheng, F.; Zhu, G.; Wang, C.; Yang, Z.; Lyu, Y. Influence of geometric parameters on the performance of ejector used in aeroengine air system. *Therm. Sci. Eng. Prog.* **2023**, *37*, 101571. [CrossRef]
2. Zhang, J.-Y.; Wang, C.; Yang, S.; Cheng, F.-N.; Geng, J.X.; Yang, Z.X.; Lyu, Y.W.; Yu, L. Research on Performance of Multi-nozzle Ejector for Aero-engine Air System. *Therm. Sci. Eng. Prog.* **2023**, *38*, 101651. [CrossRef]
3. Braimakis, K. Solar ejector cooling systems: A review. *Renew. Energy* **2021**, *164*, 566–602. [CrossRef]
4. Braccio, S.; Guillou, N.; Le Pierrès, N.; Tauveron, N.; Phan, H.T. Mass-flowrate-maximization thermodynamic model and simulation of supersonic real-gas ejectors used in refrigeration systems. *Therm. Sci. Eng. Prog.* **2023**, *37*, 101615. [CrossRef]
5. Zhu, Y.; Wang, Z.; Yang, Y.; Jiang, P.X. Flow Visualization of Supersonic Two-phase Transcritical Flow of CO_2 in an Ejector of a Refrigeration System. *Int. J. Refrig.* **2017**, *74*, 354–361. [CrossRef]
6. Ünal, S.; Cihan, E.; Erdinç, M.T.; Bilgili, M. Influence of mixing section inlet and diffuser outlet velocities on the performance of ejector-expansion refrigeration system using zeotropic mixture. *Therm. Sci. Eng. Prog.* **2022**, *33*, 101338. [CrossRef]
7. Bharate, G.; Kumar, R.A. Starting transients in second throat vacuum ejectors for high altitude testing facilities. *Aerosp. Sci. Technol.* **2021**, *113*, 106687. [CrossRef]
8. Lijo, V.; Kim, H.D.; Matsuo, S.; Setoguchi, T. A study of the supersonic ejector–diffuser system with an inlet orifice. *Aerosp. Sci. Technol.* **2012**, *23*, 321–329. [CrossRef]

9. Karthick, S.K.; Rao, S.M.V.; Jagadeesh, G.; Reddy, K.P.J. Experimental parametric studies on the performance and mixing characteristics of a low area ratio rectangular supersonic gaseous ejector by varying the secondary flow rate. *Energy* **2018**, *161*, 832–845. [CrossRef]
10. Kuo, J.K.; Wu, P.R.; Yang, T.F.; Yan, W.M. Optimal technical analysis of vacuum ejector for passive hydrogen recovery. *Int. J. Hydrog. Energy* **2023**, *48*, 8260–8272.
11. Li, Y.; Shen, S.; Niu, C.; Mu, X.; Zhang, L. The effect of variable motive pressures on the performance and shock waves in a supersonic steam ejector with non-equilibrium condensing. *Int. J. Therm. Sci.* **2023**, *185*, 108034. [CrossRef]
12. Śmierciew, K.; Butrymowicz, D.; Karwacki, J.; Bergander, M.J.; Gagan, J. Design, fabrication, and investigations of prototype supersonic micro-ejector for innovative cooling system of electronic components. *Int. J. Refrig.* **2023**, *153*, 323–336. [CrossRef]
13. Barber, T.J.; Anderson, O.L. Computational Study of a Supersonic Mixer-ejector Exhaust System. *J. Propuls. Power* **1992**, *8*, 927–934. [CrossRef]
14. Tyagi, R.K.; Rajesh, R.; Singhal, G.; Mainuddin; Dawar, A.L.; Endo, M. Parametric studies of a supersonic COIL with angular jet singlet oxygen generator. *Infrared Phys. Technol.* **2003**, *44*, 271–279. [CrossRef]
15. Tyagi, R.K.; Rajesh, R.; Singhal, G.; Mainuddin; Dawar, A.L.; Endo, M. Supersonic COIL with angular jet singlet oxygen generator. *Opt. Laser Technol.* **2003**, *35*, 395–399. [CrossRef]
16. Singhal, G.; Mainuddin; Rajesh, R.; Tyagi, R.K.; Dawar, A.L. Supersonic diffuser for pressure recovery in SCOIL system. *Opt. Laser Technol.* **2010**, *42*, 219–224. [CrossRef]
17. Opgenorth, M.J.; Sederstrom, D.; McDermott, W.; Lengsfeld, C.S. Maximizing pressure recovery using lobed nozzles in a supersonic ejector. *Appl. Therm. Eng.* **2012**, *37*, 396–402. [CrossRef]
18. Chen, J.; Wang, Z.; Wu, J.; Xu, W. Investigation on the pressure matching performance of the constant area supersonic-supersonic ejector. *Therm. Sci.* **2015**, *19*, 631–643. [CrossRef]
19. Petrovic, A.; Jovanovic, M.Z.; Genic, S.; Bugaric, U.; Delibasic, B. Evaluating performances of 1-D models to predict variable area supersonic gas ejector performances. *Energy* **2018**, *163*, 270–289. [CrossRef]
20. Hanafi, A.S.; Mostafa, G.M.; Waheed, A.; Fathy, A. 1-D Mathematical Modeling and CFD Investigation on Supersonic Steam Ejector in MED-TVC. *Energy Procedia* **2015**, *75*, 3239–3252. [CrossRef]
21. Rao, S.M.V.; Jagadeesh, G. Novel Supersonic Nozzles for Mixing Enhancement in Supersonic Ejectors. *Appl. Therm. Eng.* **2014**, *71*, 62–71. [CrossRef]
22. Eames, I.; Aphornratana, S.; Haider, H. A theoretical and experimental study of a small-scale steam jet refrigerator. *Int. J. Refrig.* **1995**, *18*, 378–386. [CrossRef]
23. Yadav, S.K.; Pandey, K.M.; Kumar, V.; Gupta, R. Computational analysis of a supersonic two-stage ejector. *Mater. Today Proc.* **2021**, *38*, 2700–2705. [CrossRef]
24. Kumar, V.; Singhal, G.; Subbarao, P.M.V. Study of supersonic flow in a constant rate of momentum change (CRMC) ejector with frictional effects. *Appl. Therm. Eng.* **2013**, *60*, 61–71. [CrossRef]
25. Lamberts, O.; Chatelain, P.; Bartosiewicz, Y. Numerical and experimental evidence of the Fabri-choking in a supersonic ejector. *Int. J. Heat Fluid Flow* **2018**, *69*, 194–209. [CrossRef]
26. Ye, W.; Zhang, J.; Xu, W.; Zhang, Z. Numerical investigation on the flow structures of the multi-strut mixing enhancement ejector. *Appl. Therm. Eng.* **2020**, *179*, 115653. [CrossRef]
27. Chong, D.; Hu, M.; Chen, W.; Wang, J.; Liu, J.; Yan, J. Experimental and numerical analysis of supersonic air ejector. *Appl. Energy* **2014**, *130*, 679–684. [CrossRef]
28. Rizzo, F.; D'Alessandro, V.; Montelpare, S.; Giammichele, L. Computational study of a bluff body aerodynamics: Impact of the laminar-to-turbulent transition modeling. *Int. J. Mech. Sci.* **2020**, *178*, 105620. [CrossRef]
29. Chong, D.; Yan, J.; Wu, G.; Liu, J. Structural optimization and experimental investigation of supersonic ejectors for boosting low pressure natural gas. *Appl. Therm. Eng.* **2009**, *29*, 2799–2807. [CrossRef]
30. Bouhanguel, A.; Desevaux, P.; Gavignet, E. Flow visualization in supersonic ejectors using laser tomography techniques. *Int. J. Refrig.* **2011**, *34*, 1633–1640. [CrossRef]
31. Zhang, H.; Wang, L.; Jia, L.; Zhao, H.; Wang, C. Influence investigation of friction on supersonic ejector performance. *Int. J. Refrig.* **2018**, *85*, 229–239. [CrossRef]
32. El Zohbi, B.; Bukharin, N.; Assoum, H.H.; Abed-Meraim, K.; Sakout, A.; El Hassan, M. Investigation of the effects of the jet nozzle geometry and location on the performance of supersonic fluid ejectors. *Energy Rep.* **2022**, *8*, 228–233. [CrossRef]

Disclaimer/Publisher's Note: The statements, opinions and data contained in all publications are solely those of the individual author(s) and contributor(s) and not of MDPI and/or the editor(s). MDPI and/or the editor(s) disclaim responsibility for any injury to people or property resulting from any ideas, methods, instructions or products referred to in the content.